Technical Note

Evaluating Sentinel-2 for Monitoring Drought-Induced Crop Failure in Winter Cereals

Adrià Descals [1,2,*], **Karen Torres** [1,2], **Aleixandre Verger** [1,2,3] and **Josep Peñuelas** [1,2]

[1] Centre de Recerca Ecològica i Aplicacions Forestals, 08193 Barcelona, Spain; k.torres@creaf.uab.cat (K.T.); a.verger@creaf.cat (A.V.); josep.penuelas@creaf.cat (J.P.)
[2] Global Ecology Unit CREAF-CSIC-UAB, 08193 Barcelona, Spain
[3] Centro de Investigaciones sobre Desertificación, CSIC-UV-GV, 46113 València, Spain
[*] Correspondence: a.descals@creaf.uab.cat

Abstract: Extreme climate events can threaten food production and disrupt supply chains. For instance, the 2023 drought in Catalonia caused large areas of winter cereals to wilt and die early, yielding no grain. This study examined whether Sentinel-2 can detect total crop losses of winter cereals using ground truth data on crop failure. The methodology explored which Sentinel-2 phenological and greenness variables could best predict three drought impact classes: normal growth, moderate impact, and high impact, where the crop failed to produce grain. The results demonstrate that winter cereals affected by drought exhibit a premature decline in several vegetation indices. As a result, the best predictors for detecting total crop losses were metrics associated with the later stages of crop development. Specifically, the mean Normalized Difference Vegetation Index (NDVI) for the first half of May showed the highest correlation with drought impact classes ($R^2 = 0.66$). This study is the first to detect total crop losses at the plantation level using field data combined with Sentinel-2 imagery. It also offers insights into rapid monitoring methods for crop failure, an event likely to become more frequent as the climate warms.

Keywords: crop failure; agricultural drought; total crop loss; winter cereals; Sentinel-2

1. Introduction

Climate change has impacted cereal crop yields, reducing global wheat production by 5.5% since 1980 [1]. Specifically, drought directly affects plant and grain growth development, leading to reduced grain yields [2]. As an example, drought conditions were particularly severe in the Mediterranean basin in 2023, affecting winter cereals and resulting in a high likelihood of crop failures [3]. As the climate warms, these extreme drought events are expected to increase in the region [4], highlighting the potential impacts of droughts on food security and food supply chains. Addressing these impacts requires the monitoring of crop production at the regional and global scale [5].

Monitoring crop failure due to extreme droughts is critical for ensuring food security, managing water resources, and mitigating economic losses [6,7]. Effective drought monitoring helps predict crop failures, allowing for proactive measures to secure food supplies and manage resources more efficiently [8,9]. In addition, monitoring the impacts of drought on crop production helps in planning and implementing financial aid and insurance schemes for affected farmers [10,11]. Thus, the early monitoring and prediction of potential drought impacts on crop production are crucial, and tools that improve the accuracy and timeliness of these monitoring systems are necessary.

Satellite remote sensing has been extensively used to monitor cereal crops and assess drought-related yield losses [12]. Various vegetation indices combined with climate data are used to monitor crop production [13–15]. In addition, phenology metrics have demonstrated their effectiveness in monitoring the impacts of drought on crop yields, as suboptimal crop growth rates are reflected in an anomalous land surface phenology observed from satellites [16,17]. These remote sensing data are often integrated with crop growth and machine learning models that enhance the accuracy of yield predictions [18,19]. Moreover, recent studies have utilized phenological metrics derived from Sentinel-2 to enhance wheat yield estimates [20,21] and other crop types [22,23]. Sentinel-2 is particularly valuable due to its high spatial resolution (10 m), which enables the monitoring of small plantations and the crop production within them [24]. These studies, however, have a limitation: they estimate drought-induced yield losses but overlook the occurrence of total crop failures caused by extreme drought events. Total crop losses occur when extreme drought conditions completely desiccate the crop, resulting in no harvestable yield. The use of remote sensing to monitor these complete crop failures remains unexplored. Given that climate change is expected to increase the frequency of extreme droughts and consequent total crop losses [7], it is important to investigate the potential use of remote sensing for monitoring crop failures.

The aim of this study is to determine whether satellite remote sensing can detect drought-induced crop failure in winter cereals and identify the key variables from Sentinel-2 data that best predict crop failure. This not only entails estimating yield, but rather the complete failure of cereal plantations due to drought. To achieve this, we collected field data on winter cereals in Catalonia, an area that experienced a severe drought in 2023. Then, we extracted phenology metrics from different Sentinel-2 vegetation indices and evaluated the relevance of these variables in predicting crop failure. The purpose of this approach is to develop a reliable method that uses the best predictors from Sentinel-2 data to monitor crop failure.

2. Materials and Methods

2.1. Study Area

We collected field data within a 1000 ha study area, which encompassed several municipalities in Catalonia. Winter cereals, which include wheat, barley, oat, and triticale, are the predominant crop in this region. Farmers sow these cereals in January and February, cultivate them from March to May, and harvest them in late May and June. The region has a Mediterranean climate, with hot and dry summers that make irrigated crops the only viable option for cultivation in summer. The average annual rainfall is 660 mm, and it usually falls in spring and autumn. Winter cereals are primarily rainfed, with the exception of cereals that are irrigated near rivers and areas with a high water table. Irrigated plantations also cultivate summer crops, primarily maize. The area is covered by family-owned smallholders with properties that rarely exceed 30 hectares. We collected all sampled points in smallholder plantations; the average plantation area was 18.7 ha, with the smallest and largest plantation areas being 0.3 ha and 26.3 ha.

The area experienced a severe drought during the first half of 2023, particularly in March and April during crucial cereal growing stages. According to the ERA5 dataset [25], the rainfall in March 2023 was only 3 mm in the study area, while the long-term (1980–2023) rainfall was 56 mm. The rainfall in April 2023 was 33 mm, while the long-term rainfall was 71 mm. Furthermore, sparse precipitation fell in late April, during the final stages of crop development. As a result, cereals received little to no rainfall during their growth stages.

2.2. Overview of the Methodology

The methodology aims to identify the most effective Sentinel-2 predictor of crop failure in the study area and evaluate its ability to explain interannual variations in cereal yield across Catalonia (Figure 1). The process begins by extracting phenological and greenness variables from the Sentinel-2 time series. Next, a Random Forest model is fitted, using each Sentinel-2 variable as the input and field data on cereal crop failure as the response variable. The best predictor of crop failure is selected based on Kendall's correlation. This predictor is then used in the Random Forest model to create a crop failure map for the study area.
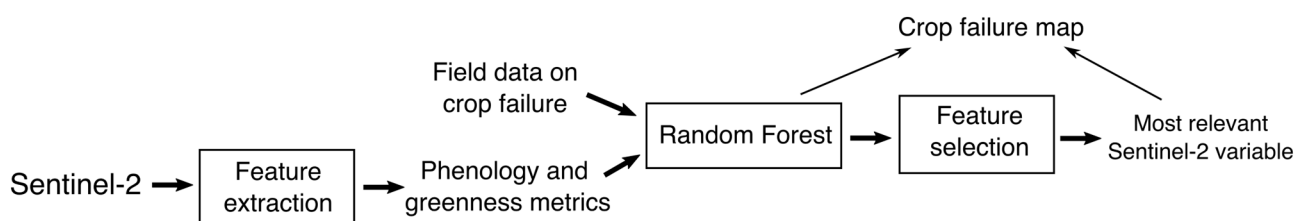

Figure 1. Flowchart of the methodology.

2.3. Collection of Field Data

We conducted field observations to obtain ground truth information on crop failure in the study area. The field data consisted of geolocated points that included information on drought affection. Data collection included visits to plantations where winter cereals were grown during the 2023 campaign. The plantations were visited between 20 April and 27 April 2023, when the impacts of the drought were clearly visible in the development stages of the plants. In these plantations, we visually inspected the plantation status and assigned three drought impact classes (Figure 2):

- Class 1—High drought impact: Plants appeared fully desiccated, exhibiting a complete yellow discoloration. The plants showed no signs of flowering and, thus, no grain was expected. This class represents plantations with total crop losses.
- Class 2—Moderate drought impact. Most of the plants appeared desiccated, yet signs of flowering stages were evident and reduced grain yield was expected.
- Class 3—Normal growth. No signs of drought impact were detected.
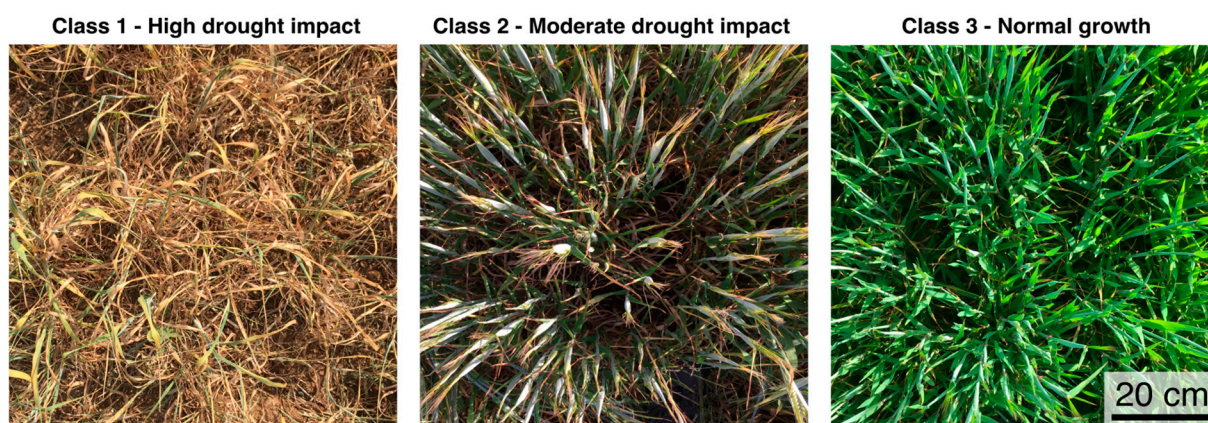
Figure 2. Three images taken during the field visits on 20 April 2023. The images show cereal plantations affected by different degrees of drought.

A total of 130 field observations were collected across the study area (Figure 3). The crops in most of the plantations showed clear signs of desiccation; 76 points were collected for class 1 (high drought impact), 28 for class 2 (moderate drought impact), and 26 for class

3 (normal growth). We found evidence of irrigation, such as pipes and water canals, in the 26 plantations that were growing without signs of drought impact. These plantations were also close to rivers with a high water table. Since drought affected all rainfed crops, irrigated crops served as a benchmark for crop growth under non-water-stress conditions. Including both irrigated and rainfed crops captures a wide range of growth conditions, which enables the identification of the Sentinel-2 variables that distinguish between drought impact classes.
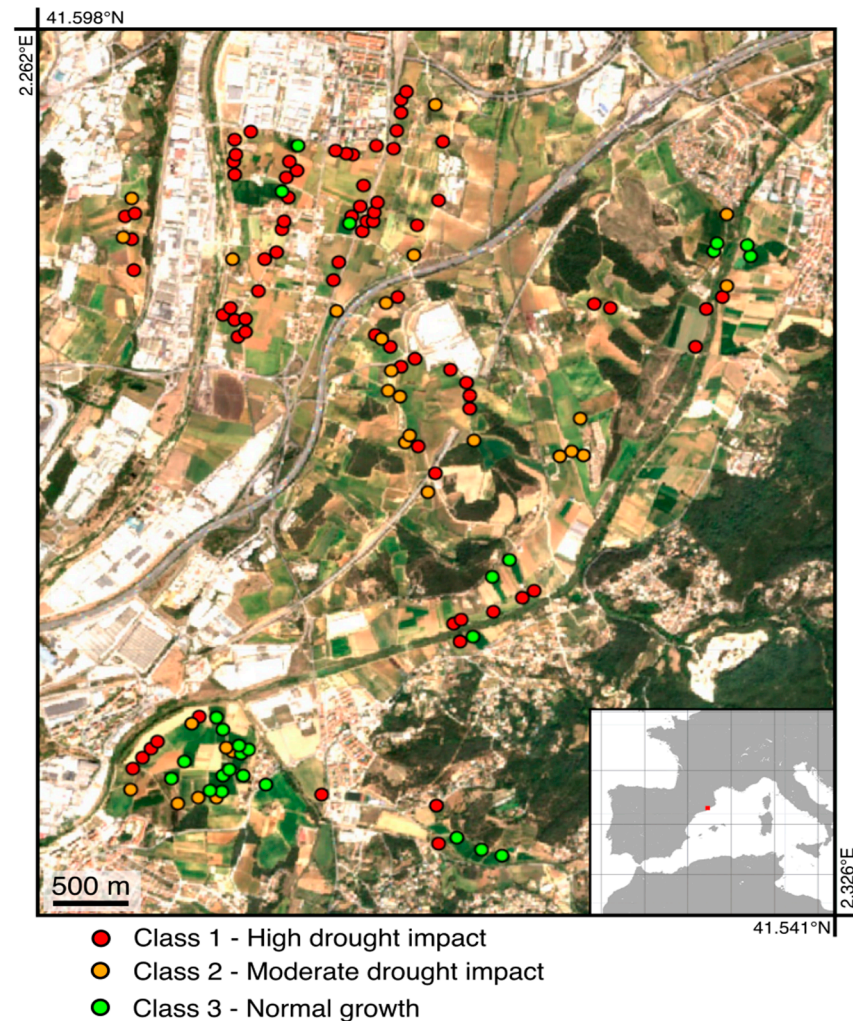
Figure 3. Location of the 130 field observations in the study area. The study area covers an area of 1000 ha near Barcelona, covering winter cereals in a Mediterranean climate region. The red dot in the inset shows the location of the study area.
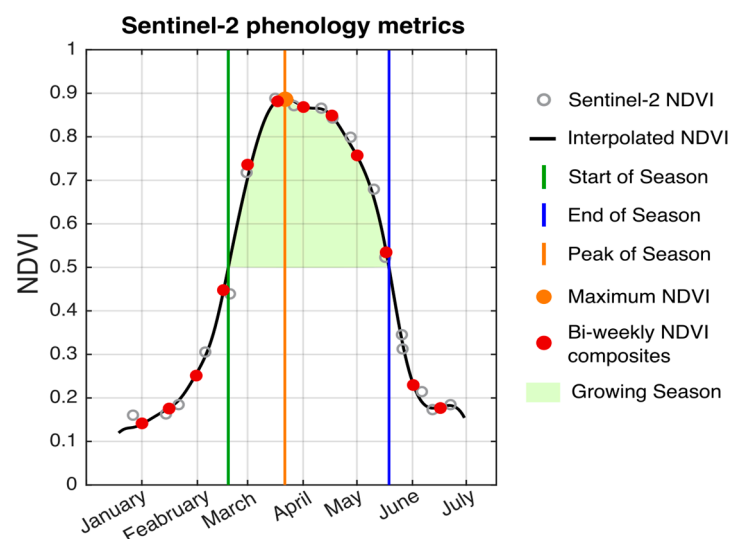
2.4. Sentinel-2 Time Series

We used Sentinel-2 data to examine the seasonality of vegetation indices, assess the so-called land surface phenology, and determine whether the seasonality differed between the three drought classes. Specifically, we used the Sentinel-2 Level-2A product [26], which includes atmospherically corrected top-of-canopy reflectance. Sentinel-2 has a spatial resolution of 10 m and a revisit time of five days, allowing the monitoring of changes in leaf phenology within the plantation [24]. All Sentinel-2 data for 2023 were extracted for the ground truth locations; specifically, the Sentinel-2 time series was extracted for the pixels that overlap with the geolocated point. In addition, we tested whether using a window size would yield different results. To do that, we also extracted the Sentinel-2 time series for a window size of 60 m (6 × 6 pixel size window for 10 m resolution bands and 3 × 3 pixel

size for 20 m resolution bands). The central pixel covered the geolocated point where we collected field information on drought impact classes. The values in the 60 m window were averaged into one single value using the mean. We masked invalid observations such as clouds and cirrus using the Scene Classification Layer present in the Level-2A product. Finally, we calculated a selection of vegetation indices derived from Sentinel-2 data, specifically the Normalised Difference Vegetation Index (NDVI), Enhanced Vegetation Index (EVI), Soil Adjusted Vegetation Index (SAVI) [27], the Red–Green Vegetation Index (RGVI) [28], and the Normalized Difference Moisture Index (NDMI) [29].

2.5. Feature Extraction

We employed feature extraction techniques to derive temporally explicit variables from Sentinel-2 vegetation indices that can potentially explain the differences among drought impact classes (Figure 4). This process involved generating metrics that captured the vegetation dynamics in response to drought events. First, we computed 15-day composites (COMP), which entailed the mean values for each vegetation index during the first and second halves of each month from January to June. This resulted in 12 variables. Then, from the 15-day aggregates, we used a cubic interpolation [30] to obtain the daily values of each vegetation index. From the interpolated daily time series, we estimated the following variables:

- Start and End of Season (SoS and EoS): These metrics indicate the onset and end of the growing season, respectively. They represent the dates when vegetation activity begins to increase (start of season) and decline (end of season), indicating the transition from dormancy to active growth, and vice versa. The phenology method used for calculating the SoS and EoS was the maximum separation method [31], which is a phenology extraction method based on thresholds. The method consists of three steps that are represented in Figure S1:

Figure 4. Phenology metrics extracted from the Sentinel-2 NDVI time series. The bi-weekly composites are 15-day aggregates of the interpolated vegetation index.

Step 1—a dynamic threshold value is defined for each site using a percentage of the amplitude in the interpolated time series (Figure S1a) (Equation (1)):

$$th = p(maxVI - minVI) + minVI \tag{1}$$

where *th* is the threshold value, *p* is a percentage, and *maxVI* and *minVI* represent the maximum and minimum vegetation index. The threshold is dynamic because it is determined by a percentage *p* of the amplitude (*maxVI–minVI*), which depends on the site and year. In this study, we calculated the SoS and EoS for the year 2023. We used a set of percentages, ranging from 10% to 90%, in steps of 10%. This resulted in 9 SoS and EoS metrics in each site.

Step 2—the interpolated time series was converted into a binary time series (Figure S1b). We represent the binary time series as *b*. Values of *b* equal to 0 (b_0) represent vegetation index observations that are lower than the threshold value *th*. In contrast, *b* values equal to 1 (b_1) are vegetation index observations that are above *th*. In this binary time series, b_1 represents observations taken during the growing season.

Step 3—the method runs a moving window with a size of 30 days for each day of 2023. In each day, we computed the ratio of b_1 observations out of all observations. This ratio was calculated for the 15 days before and after the central day; then, we calculated the difference in ratios (Equation (2)):

$$d = \sum b_{1before}/n_{before} - \sum b_{1after}/n_{after} \tag{2}$$

where n_{before} and n_{after} represent the number of observations before and after the central day of the moving window. This generates a new time series (Figure S1c) whose minimum and maximum values represent the SoS and EoS, respectively. The start of season (SoS) corresponds to the day on which the change in ratios before and after is minimal. In the SoS, the number of values above the threshold is close to zero before the central day of the window, while most values after the central day exceed the threshold. This method ensures that short lapses of regreening after the EoS are not included as part of the growing season.

- Peak of Season date (PoS): This metric refers to the date on which the vegetation index reaches its maximum during the growing season. The peak of season represents the day of highest vegetation greenness in the interpolated time series.
- Maximum Vegetation Index: This determines the highest value observed in a vegetation index (such as NDVI, EVI, or SAVI) during the growing season. It represents the maximum level of greenness observed in the interpolated time series.
- Growing Season Area (GSA): This metric represents the sum of the daily values during the period when vegetation experiences growth. The period of growth was defined as the lapse of time between the SoS and EoS calculated with a 50% threshold. The growing season area is a proxy of the total productivity of the vegetation for a given pixel.

The variables representing specific points in the Sentinel-2 time series are phenological metrics. These variables include the SoS, EoS, and PoS. In contrast, the variables indicating the magnitude of a vegetation index are greenness metrics, such as 15-day composites, the Maximum Vegetation Index, and GSA.

2.6. Feature Selection

We used the single-variable prediction [32] to identify the most important Sentinel-2 variables, i.e., features that discriminate between the drought impact classes. Single-variable prediction evaluates the model performance when only one feature is used at a time. To perform the single-variable prediction, we trained multiple Random Forest models, each using a single feature, and evaluated the model's performance. A high performance suggests a strong relevance for that particular Sentinel-2 variable. We chose Random Forests [33] because they are widely used, robust machine learning models that reduce overfitting by combining predictions from multiple decision trees. The input data for the

Random Forest models were the phenological and greenness variables extracted from the Sentinel-2 time series for 130 field locations. The predicted variable was the three drought impact classes observed during field visits. The training of the Random Forest consisted of a 5-fold cross validation; in each iteration, four folds were used for training and one fold was used for testing. To evaluate the predictive capacity of each feature, we used Kendall's correlation coefficient. We predicted the drought impact classes in the test partition and compared them to the observed classes from the field visits using Kendall's correlation to assess performance. The correlation that we report is the average obtained from the five partitions. We used Kendall's correlation because it is a non-parametric measure that evaluates the ordinal association between two variables. This makes it a good metric for determining the relationship between the predicted variable (drought impact classes) and the observed features (phenology metrics extracted from Sentinel-2). In addition to Kendall's correlation, we also evaluated the performance of the Random Forest using the overall accuracy. This metric represents the percentage of observations that have been correctly classified in the test partition.

3. Results

The field observations confirmed claims made by farmer organizations in the media: winter cereals failed to grow due to the severe drought. No pathology that could explain the death of the winter cereal crops was found during the field visits. Our inspection revealed fully desiccated plants, with no signs of mould, fungi, or other diseases typically seen on cereal leaves. Such diseases usually occur during wet and rainy seasons, when high humidity promotes their proliferation [34]. However, the study year experienced abnormally dry conditions, ruling out disease as a factor in crop failure.

The NDVI time series revealed that the three drought impact classes show a similar seasonality at the beginning of the growing season (Figure 5). This suggests that the effects of drought were not apparent in the early stages of crop development. The main differences among the classes occurred in the second half of the growing season. Class 1 showed a substantial decrease in NDVI values in April. Although class 2 does not show a substantial decrease in NDVI values, the NDVI values remain low compared to class 3. The maximum NDVI values for classes 1, 2, and 3 were 0.76, 0.80 and 0.91, respectively, suggesting that the crop growth in classes 1 and 2 did not reach the full potential growth reached in class 3.
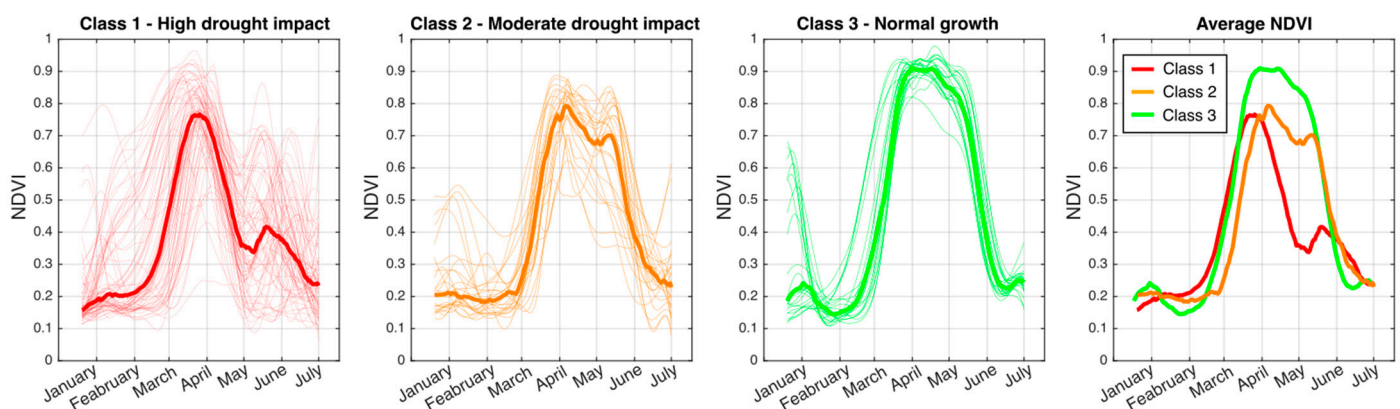

Figure 5. Sentinel-2 NDVI time series for the three classes of drought impact on winter cereal development; high drought impact, moderate drought impact, and normal crop growth. Thin lines represent the NDVI time series of individual plantations where field measurements were collected and thick lines show the average NDVI values across plantations.

We also found that some plantations showed a second peak in NDVI values during the late stages of the growing season, particularly in class 1. This increase in NDVI values was

not related to the re-greening of the crops. This re-greening was caused by the small amount of rainfall that occurred at the end of April, which encouraged the growth of weeds in the failed crops. By the time of the field visit (20–27 April), plantations classified as Class 1 had wilted and become completely desiccated, as indicated by the relative minimum NDVI values. Some field plots in Class 3 showed high NDVI values during the first weeks of the year, before winter cereals were sown. These high values correspond to the fallow vegetation that grows during the cold winter weeks. Farmers harvest the fallow and plough the land just before planting winter cereals, explaining the sharp decrease in NDVI values and subsequent increase from January to March.

We found that COMPMay1 and COMPApr2 (Kendall's correlations of 0.66 and 0.63, respectively) were the best predictors of the impact of drought (Figure 6). These were the NDVI composites for the first half of May and the second half of April, respectively. This verifies what we observed in the NDVI time series (Figure 5): drought induced substantial differences in the NDVI values among classes during the second half of the crop growing season. In contrast, the NDVI composites for the first half of the crop growing season showed a low Kendall's correlation with drought, indicating that the three classes have similar NDVI values during the first stages of plant development. Among the phenology metrics, EoS80 (i.e., the EoS computed using a threshold of 80%) showed the highest Kendall's correlation, followed by GSA, PoS, and maxVI. The high importance of EoS metrics further suggests that differences between the drought impact classes were primarily manifested in the later stages of plant development.
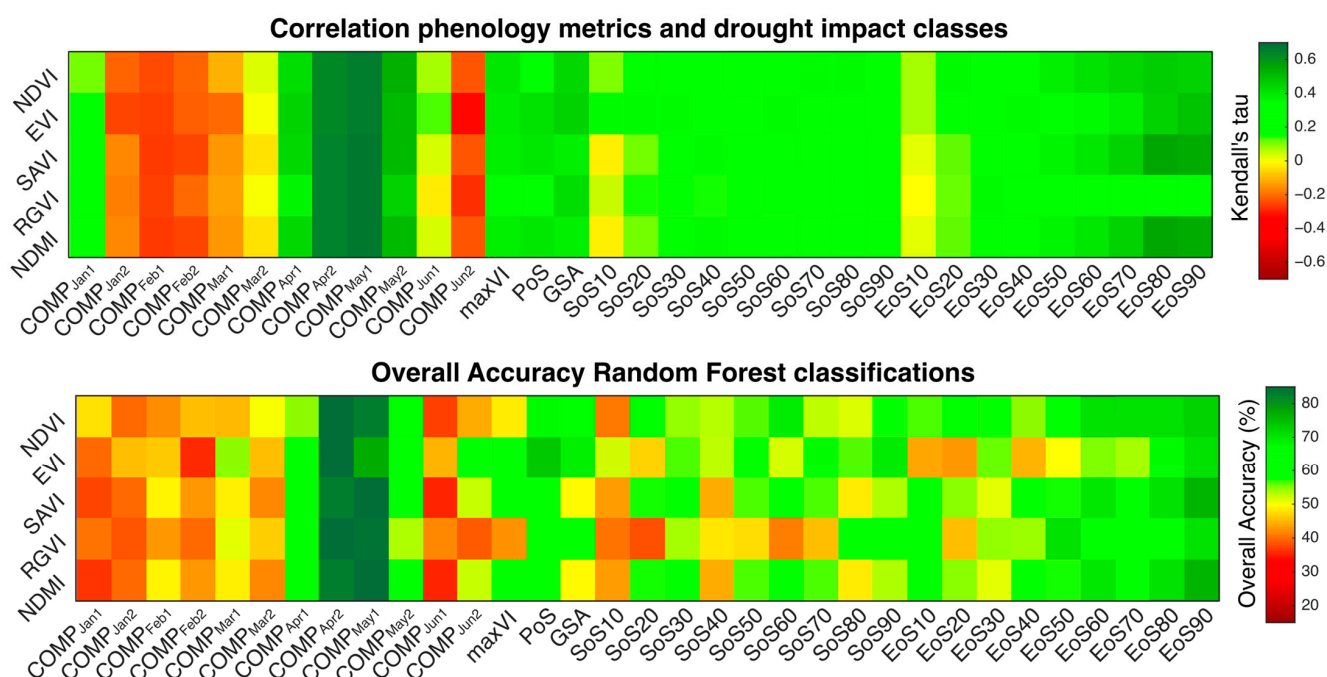
Figure 6. Results of the feature selection by vegetation index. The feature selection method was the single prediction model, in which Kendall's correlation and the overall accuracy were evaluated for each Sentinel-2 variable. Kendall's correlation was calculated between the variables extracted from different Sentinel-2 vegetation indices (NDVI, EVI, SAVI, RGVI and NDMI) and the drought classes. The overall accuracy was evaluated between the drought impact classes observed in the field and predicted in the Random Forest models. The variables are composite aggregates every 15 days (COMP), the peak of season (PoS), the growing season area (GSA), the maximum value of the vegetation index (maxVI), and the start and end of season (SoS and EoS) calculated at different thresholds (10:10:90%).

Kendall's correlation did not differ substantially among the vegetation indices. Kendall's correlation calculated with other vegetation indices also gave high importance to the variables associated with the later stages of crop development (Figure 6). In addition, the highest Kendall's correlation was found for COMPMay2; the correlations were 0.66, 0.66, 0.67, 0.67, and 0.67 for NDVI, EVI, SAVI, RGVI, and NDMI, respectively. This indicates that crop failure can be detected using a wide range of vegetation indices. The results based on overall accuracy were consistent with those obtained using Kendall's correlation. The best predictors of drought impact classes were COMPMay1 and COMPApr2, with overall accuracies of 78.6% and 68.3%, respectively, for NDVI. The results did not change when using a 60 m window size to extract Sentinel-2 data (Figure S2).

These results are important because we can predict the impact of drought on winter cereals at a regional scale using key phenological metrics. As an example, the Sentinel-2 NDVI during the second half of the first half of May 2023 was used to predict the effects of drought in the surroundings of the study area for the year 2023 (Figure 7).
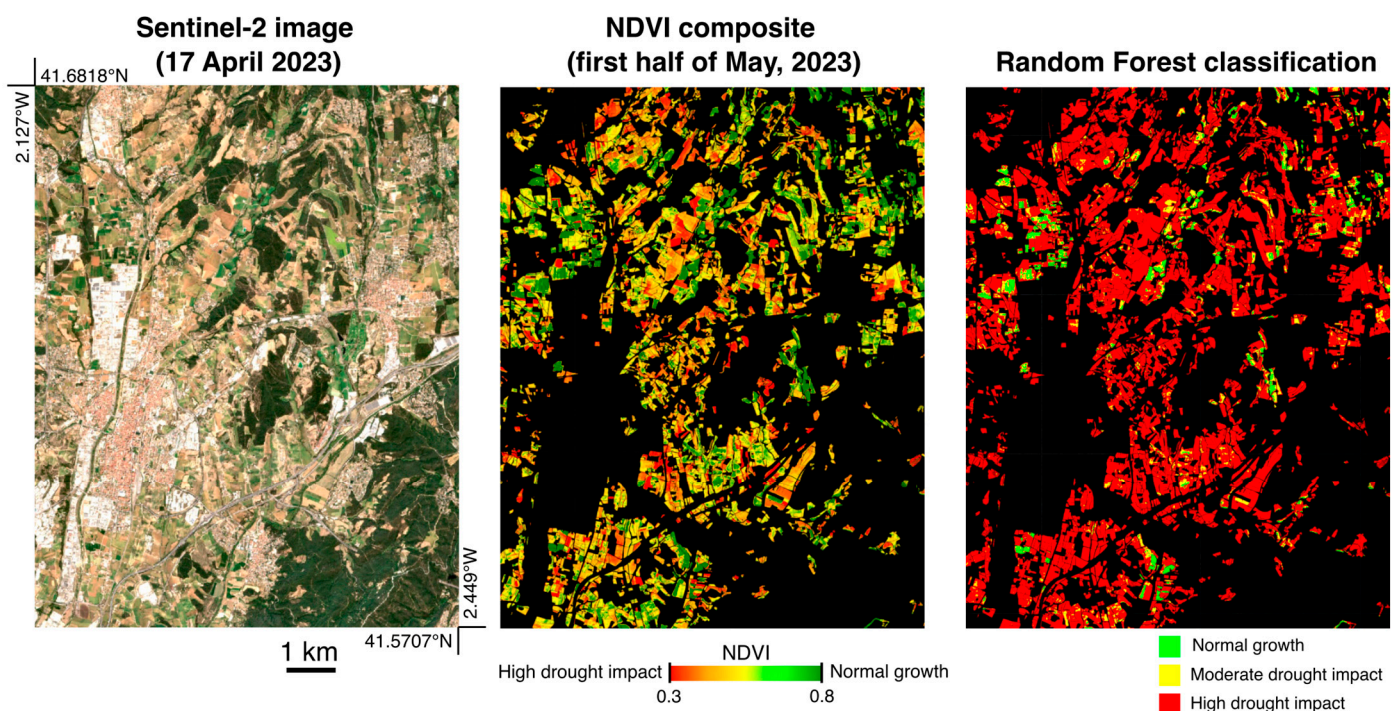
Figure 7. The map of the Normalized Difference Vegetation Index (NDVI) for the first half of May 2023 and the Random Forest classification indicating the three drought impact classes in the proximity of the study area. Non-crop pixels have been masked to focus on the agricultural areas. Kendall's correlation between the NDVI and field observations of the three drought impact classes is 0.66.

4. Discussion

A severe drought caused crop failure in winter cereals in the study area in 2023. We observed this event during our field visits and through satellite observations. The plantations that suffered crop failures showed a premature decline in Sentinel-2 NDVI, which started in early April. Our results show that extracting phenological and greenness information from Sentinel-2 during the second half of crop development is key to evaluating the impacts of drought on winter cereals. Specifically, the vegetation indices values during early May showed the highest correlation with the drought impact classes. This evidences the importance of satellite remote sensing during the later stages of crop development for monitoring drought-induced crop failure.

Crop failure may become more frequent as the climate changes, making crop yields more vulnerable to extreme events [1,7]. The period that we studied coincided with an extreme drought in the region [3]. We found that all rainfed crops suffered impacts from drought and that only irrigated crops presented normal growth. This evidence demonstrates the high impact of the 2023 drought and confirms that rainfed plantations are more susceptible to drought impacts [35,36].

Previous research has quantified the relationship between the impacts of drought, as measured by indices such as the NDVI [8,14,37]. However, these studies do not include plantations that failed due to severe drought. Our study identifies the key phenological stages that can be observed by using optical satellite data to effectively detect drought-induced crop failure in winter cereals. Our findings are in line with a previous study that demonstrated that soil moisture during critical growth stages such as tillering and stem elongation is crucial for yield, and that drought during these stages leads to significant yield losses [38]. Our findings are critical for the comprehensive mapping of crop failure on a large scale, which is important for ensuring food security [39]. Additionally, our results demonstrate that monitoring the impacts of drought can be achieved with minimal variables and by using a wide range of vegetation indices, facilitating the near-real-time monitoring of crop failure in winter cereals. This is the first study to detect complete crop losses at the plantation level using field data and Sentinel-2 imagery. It sheds light on the development of rapid monitoring techniques for crop failure.

Our methodology enables the near-real-time assessment of crop status. Since NDVI effectively indicates crop failure, users can simply calculate NDVI from the latest Sentinel-2 imagery to determine the impacts of drought on crops. Potential users include farmer cooperatives and agricultural government agencies requiring rapid regional crop status evaluations to guide interventions, such as targeted irrigation using tractor-transported water. Maps like the one in Figure 7 illustrate the type of near-real-time data generated, which can support the decision-making performed by agricultural institutions. These maps are straightforward to produce and do not require advanced expertise in remote sensing data processing.

Future studies should extend this analysis to other regions affected by crop failures caused by extreme droughts. Northern Africa, for example, also experienced a decline in winter cereal crop yield due to a severe drought in 2023 [40]. However, it is unclear whether this methodology will be effective in such areas. Variations in phenology may cause different months to serve as better predictors. Therefore, future research should account for regional differences in the timing of crop failure. This is important as crop regions show different phenology patterns [41]. In addition, future studies should refine the phenology extraction method to ensure broader applicability across different regions. Specifically, we observed a second peak in vegetation indices, corresponding to weed growth in failed crops. However, this second peak may not always indicate weed growth in other areas; it could instead represent crop regreening or the emergence of a second crop type.

Crop monitoring has become increasingly important as climate change intensifies its effects on agricultural yields [7]. Numerous studies have explored the use of remote sensing techniques for this purpose [42]. This research is relevant because climate extremes will have a significant impact on crop productivity. Our study contributes to this body of literature by offering a clear example of how extreme droughts can severely affect crop yields and how we can monitor the impacts of drought on crops with Sentinel-2.

5. Conclusions

Our study provides evidence of the devastating effects of extreme drought on winter cereal production in Catalonia in 2023. Through a combination of field visits and satellite remote sensing, we observed significant crop failure, particularly in rainfed crops. Our findings highlight the relevance of phenological and greenness information extracted from Sentinel-2 during the later stages of crop development, particularly in May, for evaluating the impacts of drought on winter cereals. Our study will help design better crop monitoring systems using satellite remote sensing, as it elucidates the variables underlying drought-induced crop failure.

Supplementary Materials: The following supporting information can be downloaded at: https://www.mdpi.com/article/10.3390/rs17020340/s1, Figure S1: Overview of the steps for phenology extraction using the Maximum Separation method; Figure S2: Results of the feature selection by vegetation index.

Author Contributions: Conceptualization, A.D. and J.P.; methodology, A.D. and K.T.; formal analysis, A.D. and K.T.; data curation, A.D. and K.T.; writing—original draft preparation, A.D. and K.T.; writing—review and editing, A.D., K.T., A.V. and J.P.; visualization, A.D. All authors have read and agreed to the published version of the manuscript.

Data Availability Statement: Sentinel-2 level-2A images are available at Copernicus Data Space: https://dataspace.copernicus.eu/ (accessed on 1 December 2024). SPEI data are available at https://spei.csic.es (accessed on 1 December 2024). Winter cereal yields were obtained from EU-ROSTATS at https://ec.europa.eu/eurostat (accessed on 1 December 2024). The field data collected in this study are available from the corresponding author upon reasonable request.

Conflicts of Interest: The authors declare no conflicts of interest.

References

1. Lobell, D.B.; Schlenker, W.; Costa-Roberts, J. Climate Trends and Global Crop Production since 1980. *Science* **2011**, *333*, 616–620. [CrossRef] [PubMed]
2. Gallagher, J.; Biscoe, P.; Hunter, B. Effects of Drought on Grain Growth. *Nature* **1976**, *264*, 541–542. [CrossRef]
3. Joint Research Center. Long Lasting Drought Led to Crop Failures in the Maghreb. 2023. Available online: https://joint-research-centre.ec.europa.eu/jrc-news-and-updates/crop-failures-due-drought-maghreb-2023-05-22_en#:~:text=Long%20lasting%20drought%20led%20to%20crop%20failures%20in%20the%20Maghreb,-The%20May%20edition&text=Drought%20conditions%20were%20particularly%20intense,the%20expense%20of%20primary%20production (accessed on 1 December 2024).
4. Spinoni, J.; Vogt, J.V.; Naumann, G.; Barbosa, P.; Dosio, A. Will Drought Events Become More Frequent and Severe in Europe? *Int. J. Climatol.* **2018**, *38*, 1718–1736. [CrossRef]
5. Park, S.; Im, J.; Jang, E.; Rhee, J. Drought Assessment and Monitoring through Blending of Multi-Sensor Indices Using Machine Learning Approaches for Different Climate Regions. *Agric. For. Meteorol.* **2016**, *216*, 157–169. [CrossRef]
6. Kim, W.; Iizumi, T.; Nishimori, M. Global Patterns of Crop Production Losses Associated with Droughts from 1983 to 2009. *J. Appl. Meteorol. Climatol.* **2019**, *58*, 1233–1244. [CrossRef]
7. Leng, G.; Hall, J. Crop Yield Sensitivity of Global Major Agricultural Countries to Droughts and the Projected Changes in the Future. *Sci. Total Environ.* **2019**, *654*, 811–821. [CrossRef]
8. Ghazaryan, G.; König, S.; Rezaei, E.E.; Siebert, S.; Dubovyk, O. Analysis of Drought Impact on Croplands from Global to Regional Scale: A Remote Sensing Approach. *Remote Sens.* **2020**, *12*, 4030. [CrossRef]
9. Yagci, A.L.; Di, L.; Deng, M.; Yu, G.; Peng, C. Global Agricultural Drought Mapping: Results for the Year 2011. In Proceedings of the 2012 IEEE International Geoscience and Remote Sensing Symposium, Munich, Germany, 22–27 July 2012; pp. 3764–3767.
10. Bokusheva, R.; Kogan, F.; Vitkovskaya, I.; Conradt, S.; Batyrbayeva, M. Satellite-Based Vegetation Health Indices as a Criteria for Insuring against Drought-Related Yield Losses. *Agric. For. Meteorol.* **2016**, *220*, 200–206. [CrossRef]
11. Lesk, C.; Rowhani, P.; Ramankutty, N. Influence of Extreme Weather Disasters on Global Crop Production. *Nature* **2016**, *529*, 84–87. [CrossRef] [PubMed]

12. Karmakar, P.; Teng, S.W.; Murshed, M.; Pang, S.; Li, Y.; Lin, H. Crop Monitoring by Multimodal Remote Sensing: A Review. *Remote Sens. Appl. Soc. Environ.* **2024**, *33*, 101093. [CrossRef]

13. Franke, J.; Menz, G. Multi-Temporal Wheat Disease Detection by Multi-Spectral Remote Sensing. *Precis. Agric.* **2007**, *8*, 161–172. [CrossRef]

14. Yu, H.; Zhang, Q.; Sun, P.; Song, C. Impact of Droughts on Winter Wheat Yield in Different Growth Stages during 2001–2016 in Eastern China. *Int. J. Disaster Risk Sci.* **2018**, *9*, 376–391. [CrossRef]

15. Hu, P.; Sharifi, A.; Tahir, M.N.; Tariq, A.; Zhang, L.; Mumtaz, F.; Shah, S.H.I.A. Evaluation of Vegetation Indices and Phenological Metrics Using Time-Series Modis Data for Monitoring Vegetation Change in Punjab, Pakistan. *Water* **2021**, *13*, 2550. [CrossRef]

16. Bolton, D.K.; Friedl, M.A. Forecasting Crop Yield Using Remotely Sensed Vegetation Indices and Crop Phenology Metrics. *Agric. For. Meteorol.* **2013**, *173*, 74–84. [CrossRef]

17. Chandel, N.; Tiwari, P.; Singh, K.; Jat, D.; Gaikwad, B.; Tripathi, H.; Golhani, K. Yield Prediction in Wheat (*Triticum aestivum* L.) Using Spectral Reflectance Indices. *Curr. Sci.* **2019**, *116*, 272–278. [CrossRef]

18. Evans, F.H.; Shen, J. Long-Term Hindcasts of Wheat Yield in Fields Using Remotely Sensed Phenology, Climate Data and Machine Learning. *Remote Sens.* **2021**, *13*, 2435. [CrossRef]

19. Wang, Q.; Wu, J.; Li, X.; Zhou, H.; Yang, J.; Geng, G.; An, X.; Liu, L.; Tang, Z. A Comprehensively Quantitative Method of Evaluating the Impact of Drought on Crop Yield Using Daily Multi-Scale SPEI and Crop Growth Process Model. *Int. J. Biometeorol.* **2017**, *61*, 685–699. [CrossRef] [PubMed]

20. Hunt, M.L.; Blackburn, G.A.; Carrasco, L.; Redhead, J.W.; Rowland, C.S. High Resolution Wheat Yield Mapping Using Sentinel-2. *Remote Sens. Environ.* **2019**, *233*, 111410. [CrossRef]

21. Idrissi, A.; Htitiou, A.; Nadem, S.; Boudhar, A.; Lebrini, Y.; Benabdelouahab, T. Modeling Wheat Yield by Using Phenological Metrics Derived from Sentinel-2 in Arid and Semi-Arid Regions: A Case Study in Morocco. *Afr. J. Land Policy Geospat. Sci.* **2023**, *5*, 1–18.

22. Ma, C.; Johansen, K.; McCabe, M.F. Monitoring Irrigation Events and Crop Dynamics Using Sentinel-1 and Sentinel-2 Time Series. *Remote Sens.* **2022**, *14*, 1205. [CrossRef]

23. Kayad, A.; Sozzi, M.; Gatto, S.; Marinello, F.; Pirotti, F. Monitoring Within-Field Variability of Corn Yield Using Sentinel-2 and Machine Learning Techniques. *Remote Sens.* **2019**, *11*, 2873. [CrossRef]

24. Segarra, J.; Araus, J.L.; Kefauver, S.C. Farming and Earth Observation: Sentinel-2 Data to Estimate within-Field Wheat Grain Yield. *Int. J. Appl. Earth Obs. Geoinf.* **2022**, *107*, 102697. [CrossRef]

25. Muñoz-Sabater, J.; Dutra, E.; Agustí-Panareda, A.; Albergel, C.; Arduini, G.; Balsamo, G.; Boussetta, S.; Choulga, M.; Harrigan, S.; Hersbach, H.; et al. ERA5-Land: A State-of-the-Art Global Reanalysis Dataset for Land Applications. *Earth Syst. Sci. Data Discuss.* **2021**, 1–50. [CrossRef]

26. Drusch, M.; Del Bello, U.; Carlier, S.; Colin, O.; Fernandez, V.; Gascon, F.; Hoersch, B.; Isola, C.; Laberinti, P.; Martimort, P.; et al. Sentinel-2: ESA's Optical High-Resolution Mission for GMES Operational Services. *Remote Sens. Environ.* **2012**, *120*, 25–36. [CrossRef]

27. Pamungkas, S. Analysis of Vegetation Index for Ndvi, Evi-2, and Savi for Mangrove Forest Density Using Google Earth Engine in Lembar Bay, Lombok Island. In Proceedings of the IOP Conference Series: Earth and Environmental Science, Makassar, Indonesia, 23–24 November 2023; IOP Publishing: Bristol, UK, 2023; Volume 1127, p. 012034.

28. Yin, G.; Verger, A.; Descals, A.; Filella, I.; Peñuelas, J. A Broadband Green-Red Vegetation Index for Monitoring Gross Primary Production Phenology. *J. Remote Sens.* **2022**, *2022*, 9764982. [CrossRef]

29. Gao, B.-C. NDWI—A Normalized Difference Water Index for Remote Sensing of Vegetation Liquid Water from Space. *Remote Sens. Environ.* **1996**, *58*, 257–266. [CrossRef]

30. Wongsai, N.; Wongsai, S.; Huete, A.R. Annual Seasonality Extraction Using the Cubic Spline Function and Decadal Trend in Temporal Daytime MODIS LST Data. *Remote Sens.* **2017**, *9*, 1254. [CrossRef]

31. Descals, A.; Verger, A.; Yin, G.; Peñuelas, J. A Threshold Method for Robust and Fast Estimation of Land-Surface Phenology Using Google Earth Engine. *IEEE J. Sel. Top. Appl. Earth Obs. Remote Sens.* **2020**, *14*, 601–606. [CrossRef]

32. Parr, T.; Hamrick, J.; Wilson, J.D. Nonparametric Feature Impact and Importance. *Inf. Sci.* **2024**, *653*, 119563. [CrossRef]

33. Breiman, L. Random Forests. *Mach. Learn.* **2001**, *45*, 5–32. [CrossRef]

34. Różewicz, M.; Wyzińska, M.; Grabiński, J. The Most Important Fungal Diseases of Cereals—Problems and Possible Solutions. *Agronomy* **2021**, *11*, 714. [CrossRef]

35. Jaramillo, S.; Graterol, E.; Pulver, E. Sustainable Transformation of Rainfed to Irrigated Agriculture through Water Harvesting and Smart Crop Management Practices. *Front. Sustain. Food Syst.* **2020**, *4*, 437086. [CrossRef]

36. Venkatappa, M.; Sasaki, N.; Han, P.; Abe, I. Impacts of Droughts and Floods on Croplands and Crop Production in Southeast Asia—An Application of Google Earth Engine. *Sci. Total Environ.* **2021**, *795*, 148829. [CrossRef] [PubMed]

37. Laurila, H.; Karjalainen, M.; Kleemola, J.; Hyyppä, J. Cereal Yield Modeling in Finland Using Optical and Radar Remote Sensing. *Remote Sens.* **2010**, *2*, 2185–2239. [CrossRef]

38. Benito-Verdugo, P.; Martínez-Fernández, J.; González-Zamora, Á.; Almendra-Martín, L.; Gaona, J.; Herrero-Jiménez, C.M. Impact of Agricultural Drought on Barley and Wheat Yield: A Comparative Case Study of Spain and Germany. *Agriculture* **2023**, *13*, 2111. [CrossRef]

39. Karthikeyan, L.; Chawla, I.; Mishra, A.K. A Review of Remote Sensing Applications in Agriculture for Food Security: Crop Growth and Yield, Irrigation, and Crop Losses. *J. Hydrol.* **2020**, *586*, 124905. [CrossRef]

40. Toreti, A.; Bavera, D.; Acosta, N.J.; Arias-Muñoz, C.; Barbosa, P.; De, J.A.; Di, C.C.; Fioravanti, G.; Grimaldi, S.; Hrast, E.A.; et al. *Drought in the Western Mediterranean—May 2023*; Publications Office of the European Union: Luxembourg, 2023.

41. Van Tricht, K.; Degerickx, J.; Gilliams, S.; Zanaga, D.; Battude, M.; Grosu, A.; Brombacher, J.; Lesiv, M.; Bayas, J.C.L.; Karanam, S.; et al. WorldCereal: A Dynamic Open-Source System for Global-Scale, Seasonal, and Reproducible Crop and Irrigation Mapping. *Earth Syst. Sci. Data* **2023**, *15*, 5491–5515. [CrossRef]

42. Hatfield, J.L.; Prueger, J.H.; Sauer, T.J.; Dold, C.; O'brien, P.; Wacha, K. Applications of Vegetative Indices from Remote Sensing to Agriculture: Past and Future. *Inventions* **2019**, *4*, 71. [CrossRef]